International Journal of Solids and Structures 48 (2011) 1239–1247

Contents lists available at ScienceDirect

International Journal of Solids and Structures

journal homepage: www.elsevier.com/locate/ijsolstr

On the evolution of intrinsic curvature in rod-based models of growth in long slender plant stems

O.M. O'Reilly [a,*], T.N. Tresierras [a,b]

[a] Department of Mechanical Engineering, University of California at Berkeley, Berkeley, CA 94720, USA
[b] Exponent Failure Analysis Associates, 4101 SW 71st Avenue, Miami, FL 33155, USA

ARTICLE INFO

Article history:
Received 24 July 2010
Received in revised form 4 November 2010
Available online 21 December 2010

Keywords:
Growth models
Biomechanics
Residual stress
Rod theory
Elastica

ABSTRACT

In many applications of rod theories as models for plant stem growth and development, it is necessary to allow the intrinsic curvature and flexural stiffness of the rod to evolve. In the present paper, the application of evolution equations for these quantities is examined and a new evolution equation for the intrinsic curvature is proposed. To illustrate the new evolution equation, several examples of the evolution of rods in the presence of external forces and tip growth are presented. Growth in plants frequently results in residual stresses and the compatibility of rod models with these fields is also discussed.

1. Introduction

The growth and evolution of a plant stem features several mechanical phenomena. First, as the tip grows and the stem elongates, the added weight causes the plant to become increasingly deformed. This deformation is controlled by the lateral accretion of mass on the outer surface of the stem, a possible stiffening of the stem, and the development of intrinsic curvature. These features are evident when one cuts a stem from a rose plant and notices that the shape of the stem does not change significantly after it has been cut. They can also be observed in the oscillations of plant stems which are subject to transient loading caused by wind and rain.

The use of rod theories to model plant stems has a long history which dates at least to the seminal work by Greenhill (1881) on the stability of a column. More recent works, such as those by Silk and Erickson (1980) and Silk et al. (1982) have used Euler's theory of the elastica to model the evolution of a rice panicle, Goriely and Neukirch (2006) and McMillen and Goriely (2002) have used Kirchhoff–Love rod theory to examine tendril perversion and climbing in vines of morning glories, while Yamamoto et al. (2002) have used rod theories to examine the growth of wooded plant stems. Arguably among the most ambitious works in this area are Costes et al. (2008), Fourcaud and Lac (2003) and Fourcaud et al. (2003) who model individual branches using rods and then combine the rods to form trees.

The contribution of the present paper to the literature is to present a novel evolution equation for the intrinsic curvature κ_g of a rod (see (11)). Evolution equations, or growth laws, of this type play a central role in biomechanical models for growth, and our equation for κ_g has similarities to related works on the growth development in continuum theories (see Taber (1995, 2009) and references cited therein). The Eq. (11) enables the rod to be used to model growing plant stems and we use it in conjunction with an earlier theory that we developed in Faruk Senan et al. (2008). This theory, which is based on Euler's theory of the elastica, is sufficiently general to accommodate tip growth (also known as primary growth), lateral accretion (secondary growth), an evolving intrinsic curvature κ_g, and remodeling. However, the evolution equation for κ_g that is used in Faruk Senan et al. (2008) is inadequate when there is significant tip growth. The growth law presented in this paper addresses this deficiency and we illustrate its use with a range of examples which include comparisons to earlier published works on plant stem growth modeling.

The selection of rod theories to model plant stems is an obvious choice in many respects. However, several technical difficulties quickly present themselves. One of the main issues is the development of growth strains in so-called reaction woods of wooded plant stems. These strains lead to the development of residual stresses (which are often referred to as growth stresses), and the residual stresses can be released when the plant is felled and cut into planks and often leads to distortion of the planks. There has been a considerable volume of work aimed at quantifying and modeling these residual stresses and the biochemical stimuli that control them (see Archer (1986), Fournier et al. (1990), Ormarsson

* Corresponding author. Tel.: +1 510 642 0877; fax: +1 510 643 5599.
E-mail address: oreilly@me.berkeley.edu (O.M. O'Reilly).

0020-7683/$ - see front matter © 2011 Elsevier Ltd. All rights reserved.
doi:10.1016/j.ijsolstr.2010.12.006

et al. (2009) and Wilson and Archer (1977), and references cited therein).[1] The vast majority of models use the three-dimensional theory of linear elasticity and accommodate the growth strains (swelling strains) in a manner which is similar to treatments of thermal strains in linear thermoelasticity. Although the constitutive relations we use in this paper have similarities to those used in modeling the production of growth stress in the stems of wooded plants, the one-dimensional nature of the rod theory that we use is unable to accommodate several forms of residual stress fields that have been reported for wooded plant stems. A criterion for the compatibility of the plant stem model and residual stress is developed in the Appendix A to this paper.

An outline of this paper is as follows. In the next section, several features from the rod theory developed in Faruk Senan et al. (2008) are recalled. The new evolution equation for κ_g is presented in Section 3, and the governing equations for a plant stem modeled using the rod theory are summarized in Section 4. These equations are illustrated using a range of examples in Sections 5 and 6. The paper closes with a discussion of open problems and an Appendix A on the issue of residual stresses and their counterparts in the rod theory.

2. A simple rod-based model for plant growth

In Euler's theory of the elastica (see Love, 1944), the rod is modeled as a deformable material curve $\mathcal{C}$ which resists bending. It is standard to identify $\mathcal{C}$ with the centerline of the rod-like body that this nonlinear theory of a deformable rod is modeling. In order to model plant growth using the elastica, the classical formulation needs several modifications. These modifications are discussed in Faruk Senan et al. (2008) and our summary discussion here is based on this paper.

The material points of $\mathcal{C}$ are identified by the convected coordinate ξ and we denote the end points of $\mathcal{C}$ by $\xi = \xi_A$ and $\xi = \xi_B$. In order to accommodate tip growth, the coordinates $\xi_{A,B}$ can be functions of time. We endow each point on $\mathcal{C}$ with an area a, a moment of area I, and a mass density ρ. In addition to their usual dependency on ξ (which can be attributed to geometric taper of the plant stem), a, I, and ρ are also functions of time because of tip growth and mass deposition and accretion.

To use a rod theory to model a growing plant stem, three configurations of $\mathcal{C}$ are used (cf. Fig. 1). Each of the three configurations evolve in time. In addition to the familiar reference configuration $\mathcal{L}_0$ and present configuration $\mathcal{L}$, a growth configuration $\mathcal{L}_g$ is also defined. We embed each of these configurations on a plane $\mathbb{P}$ in $\mathbb{E}^3$ which has the unit normal vector $\mathbf{e}_3$. For convenience, we assume the centerline $\mathcal{C}$ of the rod in $\mathcal{L}_0$ is straight and the coordinate ξ is the arc-length parameter in this configuration. Thus, the position vector $\mathbf{r}_0$ of a material point ξ in $\mathcal{L}_0$ has the representation

$$\mathbf{r}_0(\xi,t) = x(\xi,t)\mathbf{E}_2 + \mathbf{c}, \tag{1}$$

where $\mathbf{c}$ is a constant and $\{\mathbf{E}_1, \mathbf{E}_2, \mathbf{E}_3 = \mathbf{e}_3\}$ is a fixed right-handed Cartesian basis for $\mathbb{E}^3$.

The position vector of a material point of $\mathcal{C}$ in $\mathcal{L}$ is defined by the vector-valued function $\mathbf{r} = \mathbf{r}(\xi,t)$, and the arc-length parameter for $\mathcal{C}$ in $\mathcal{L}$ is denoted by s. The growth configuration $\mathcal{L}_g$ is attained from $\mathcal{L}$ by removing the external applied forces and moments. That is, it is the unloaded configuration at time t of the rod. The position vector of a material point in $\mathcal{L}_g$ is defined by the vector-valued function $\mathbf{r}_g = \mathbf{r}_g(\xi,t)$, and $\mathcal{C}$ in $\mathcal{L}_g$ has the arc-length parameter s_g.

[1] These works are part of an ever increasing literature on growth-induced residual stress formation in biological tissues, and we refer the interested reader to Alford et al. (2008), Fung (1991), Johnson and Hoger (1995), and references cited therein.

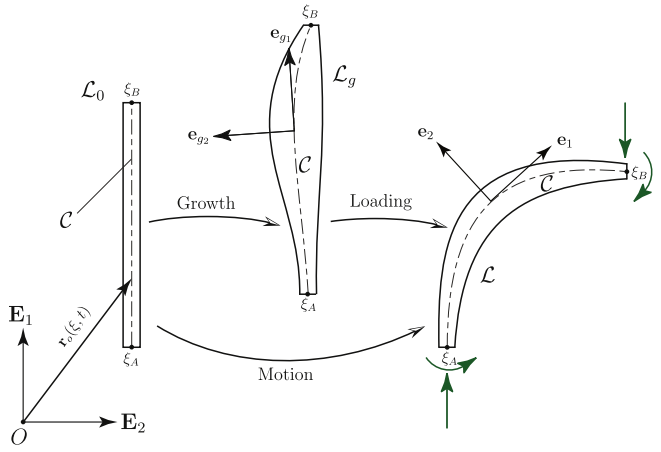

Fig. 1. The elastica is represented by the rod centerline in three configurations, $\mathcal{L}_0$, $\mathcal{L}_g$, and $\mathcal{L}$. Each centerline is a material curve $\mathcal{C}$ parameterized by the reference configuration's arc-length parameter ξ.

As illustrated in Fig. 1, it is convenient to define two triads $\{\mathbf{e}_{1_g}, \mathbf{e}_{2_g}, \mathbf{E}_3\}$ and $\{\mathbf{e}_1, \mathbf{e}_2, \mathbf{E}_3\}$ associated with $\mathcal{C}$ in $\mathcal{L}_g$ and $\mathcal{L}$, respectively:

$$\mathbf{e}_{1_g}(\xi,t) = \frac{\partial \mathbf{r}_g}{\partial s_g} = \cos(\theta_g)\mathbf{E}_1 + \sin(\theta_g)\mathbf{E}_2, \quad \mathbf{e}_{2_g}(\xi,t) = \mathbf{E}_3 \times \mathbf{e}_{1_g}(\xi,t),$$
$$\mathbf{e}_1(\xi,t) = \frac{\partial \mathbf{r}}{\partial s} = \cos(\theta)\mathbf{E}_1 + \sin(\theta)\mathbf{E}_2, \quad \mathbf{e}_2(\xi,t) = \mathbf{E}_3 \times \mathbf{e}_1(\xi,t). \tag{2}$$

In the sequel, we assume that the motion of the elastica between $\mathcal{L}_g$ and $\mathcal{L}$ does not alter the stretch of $\mathcal{C}$:

$$\frac{\partial s}{\partial s_g} = 1. \tag{3}$$

This constraint allows us to conveniently parameterize the growth and present configurations with the coordinate s. The curvatures κ_g and κ are easily defined with the help of (2):

$$\kappa_g = \frac{\partial \theta_g}{\partial s}, \quad \kappa = \frac{\partial \theta}{\partial s}. \tag{4}$$

Here, κ_g is synonymous with the intrinsic curvature of the rod. The difference in curvature between the present and growth configurations is

$$v = \kappa - \kappa_g. \tag{5}$$

In the sequel, v will be used as a strain measure.[2]

We now recall the balance laws for the modified elastica postulated in Faruk Senan et al. (2008).[3] This model captures two forms of movement: *growth-related* movement, which is a consequence of the time-related changes in material properties, and *reactionary* movement, which is due to the time rate of change of components that appear in the local form of the balance laws. The time scales of these forms of movement can differ by several orders of magnitude. In the present paper, we are only interested in growth-related movement. Consequently, we restrict attention to the quasi-static form of the balance laws:

$$\rho\mathbf{f} + \frac{\partial \mathbf{n}}{\partial s} = \mathbf{0}, \quad \frac{\partial \mathbf{m}}{\partial s} + \mathbf{m}_a + \frac{\partial \mathbf{r}}{\partial s} \times \mathbf{n} = \mathbf{0}. \tag{6}$$

[2] In many works on rod models for plant growth, such as, Alméras et al. (2002), Fourcaud and Lac (2003), and Yamamoto et al. (2002), the intrinsic curvature κ_g of the rod is not explicitly defined. However, we strongly suspect that there is a growth configuration implicit in the cited models.

[3] The development of these laws is based on the works Green and Naghdi (1995, 1979), O'Reilly (2007), O'Reilly and Varadi (2003), and Rubin (2000).

Here, $\mathbf{n}$ is a contact force, $\mathbf{m}$ is the contact moment, ρ is the mass density,[4] $\rho\mathbf{f}$ is the assigned force, and $\mathbf{m}_a$ is the assigned moment. If the rod is loaded under gravity, then we have the prescriptions

$$\rho\mathbf{f} = -\rho g\mathbf{E}_2, \quad \mathbf{m}_a = \mathbf{0}. \tag{7}$$

In order to capture intrinsic curvature, we prescribe a simple free-energy function $\rho\psi$:

$$\rho\psi = \frac{1}{2}D(\kappa - \kappa_g)^2, \tag{8}$$

where D is the bending stiffness (flexural rigidity) of the rod. As in Faruk Senan et al. (2008), a local form of the balance of energy, which we refrain from reproducing here, leads to a constitutive equation for the bending moment $\mathbf{m} = m\mathbf{E}_3$:

$$m = D\left(\frac{\partial\theta}{\partial s} - \frac{\partial\theta_g}{\partial s}\right) = D(\kappa - \kappa_g) = Dv. \tag{9}$$

The function κ_g will shortly be prescribed by a temporal evolution equation.

3. An evolution equation for the intrinsic curvature

One of the unique features of the model discussed in this paper is the intrinsic curvature κ_g. In the growth of plants, it is common for changes in the geometric and constitutive properties to occur. In addition, mass accretion and remodeling produces a change in κ_g. As discussed in Faruk Senan et al. (2008) and Goriely and Goldstein (2006), κ_g is observed to evolve in plants so that it tends to approach κ. Even for the quasistatic theory of interest, κ will also change due to tip growth. The situation is further complicated by the fact that the flexural rigidity $D = EI$ can change in two manners. The first manner is by lateral accretion of material $\dot{\mathrm{I}} \neq 0$ and the second is by a remodeling of the rod's constitutive properties $\dot{\mathrm{E}} \neq 0$.[5]

To use the plant growth model, we first need to prescribe evolution equations for $D(s,t)$, $\rho(s,t)$, and κ_g. Here, we follow Faruk Senan et al. (2008) and employ their evolution equation for $D(s,t)$:

$$\tau\dot{D} + D = i_D. \tag{10}$$

In this equation, $i_D > 0$, which is a function of $s = s_g$ and t, is the stiffness profile of the rod and $\tau > 0$ is a relaxation time. The function $\rho(s,t)$ is easy to prescribe once the taper of the plant stem has been defined. The evolution equation for κ_g is

$$D\dot{\kappa}_g = \dot{D}(\kappa - \kappa_g + \kappa_c) + D\dot{\kappa}_{g_l}. \tag{11}$$

The function $\kappa_c(s,t)$ in (11) represents an induced curvature related to the change in stiffness D and the function $\kappa_{g_l}(s,t)$ represents the curvature induced by remodeling. Both of these functions act like control inputs for the plant stem model and must be prescribed: For instance, by prescribing $\kappa_c = \kappa_g - \kappa$ and $\dot{\kappa}_{g_l} = 0$, $\kappa_g(s,t)$ will remain constant in time.

Unlike the plant's ability to change geometric and constitutive properties, the ability to control intrinsic curvature κ_g along the arc-length of the stem over time gives the plant the most versatile control over its movement. The partial differential Eq. (11) favors the evolution of $\kappa_g \to \kappa + \kappa_c$. Thus, the strain $v \to -\kappa_c$. When $\kappa_c = 0$, we have found instances of plant growth modeling where κ becomes very large because, while κ_g increases, a non-trivial moment Dv needed to support external loading must be supplied. In these situations, the plant stem droops excessively.

For future purposes, it is convenient to express (11) in an integro-differential form:

$$D(s,t)\kappa_g(s,t) = D(s,t_0)\kappa_g(s,t_0) + K_c + K_{g_l}, \tag{12}$$

where

$$\begin{aligned} K_c &= K_c(s,t,t_0) = \int_{t_0}^{t}\left[\dot{D}(s,\tau)(\kappa(s,\tau) + \kappa_c(s,\tau))\right]\mathrm{d}\tau, \\ K_{g_l} &= K_{g_l}(s,t,t_0) = \int_{t_0}^{t}\left(D(s,\tau)\dot{\kappa}_{g_l}(s,\tau)\right)\mathrm{d}\tau. \end{aligned} \tag{13}$$

Referring to (13), it is apparent that K_c quantifies the net change in the intrinsic curvature κ_g due to lateral accretion and constitutive remodeling. That is, if $\dot{D}(s,\tau) = 0$ at a particular material point, then $K_c = 0$.

3.1. Other evolution equations

To place (11) in the context of earlier evolution equations for κ_g, we note that the evolution equation for κ_g in Faruk Senan et al. (2008) was

$$D\dot{\kappa}_g = \dot{D}(\kappa - \kappa_g). \tag{14}$$

This equation was motivated by an evolution equation proposed by Goriely and Goldstein (2006):

$$\tau_{GG}\dot{\kappa}_g = \kappa - \kappa_g, \tag{15}$$

where τ_{GG} is a constant relaxation time. Clearly (14) can be obtained from (11) by setting both of the functions κ_c and κ_{g_l} to zero. Unfortunately, as mentioned in Faruk Senan et al. (2008) the evolution Eq. (14) is deficient when tip growth is present.

Under the special circumstance when

$$\kappa_{g_l} = \kappa + \kappa_c, \tag{16}$$

we can evaluate the integral in (12) with the help of (9) to obtain

$$m(s,t) - m(s,t_0) = -D(s,t)\kappa_c(s,t) + D(s,t_0)\ \kappa_c(s,t_0). \tag{17}$$

When $D\kappa_c$ is a constant function of time, (17) is equivalent to the statement that the bending moment m in the rod at each location is constant. When $\dot{\kappa} = 0$, (i.e., the centerline of the present configuration is fixed) and $\kappa_c = 0$, (17) reduces to the evolution Eq. (14) for κ_g that is used in Faruk Senan et al. (2008) and

$$K_c = (D(s,t) - D(s,t_0))\kappa(s,t_0), \quad K_{g_l} = 0. \tag{18}$$

However, when tip growth is present, we have found that even (17) does not adequately model growth phenomena.

3.2. Additional remarks on the evolution equation

To provide additional motivation for the evolution Eq. (12) (or (11)), it is instructive to consider a circular rod with a bending stiffness EI_1 and intrinsic curvature κ_{1_0}. Mimicing lateral accretion, we consider a second rod which is in the form of a hollow circular tube with a bending stiffness EI_2 and intrinsic curvature κ_{2_0}. As shown in Fig. 2, we apply bending moments to the ends of both rods and combine them together to form a composite rod.[6] After removing the terminal moments, the composite rod will have a curvature identical to its intrinsic curvature κ_0:

$$D_1(\kappa_0 - \kappa_{1_0}) + D_2(\kappa_0 - \kappa_{2_0}) = 0. \tag{19}$$

The flexural stiffness of the composite rod is $D = D_1 + D_2$.

[4] The mass density ρ is per unit length of the coordinate s for $\mathcal{C}$ in $\mathcal{L}$.

[5] Here, and in the sequel, the superposed dot, $\dot{f}$, indicates the partial derivative $\frac{\partial f}{\partial t}$ of a function $f(s,t)$ keeping s fixed.

[6] If this problem were modeled using a three-dimensional theory, then residual stresses would be present in both of the bodies when they are combined to form the composite rod. As discussed in the Appendix A, the rod theory we are using is not sufficiently sophisticated to predict these residual stresses.

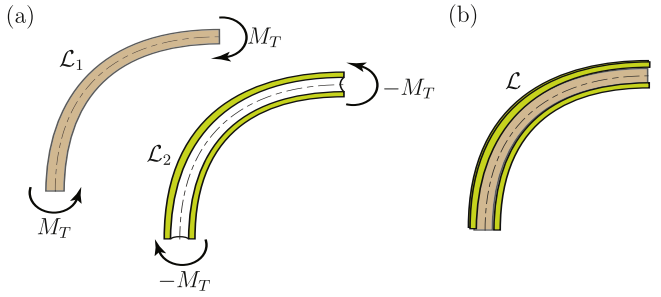

Fig. 2. The formation of a composite rod $\mathcal{L}$ from a circular rod $\mathcal{L}_1$ and a hollow rod $\mathcal{L}_2$. (a) The rods loaded with terminal moments $\pm M_T$, and (b) the composite rod.

In secondary growth of plants, material is accreted on the lateral surface and so now suppose that the second hollow rod mimics this growth:

$$D_2 = \Delta D_1, \quad \kappa_{2_0} = \kappa_{1_0} + \Delta\kappa_0, \quad \kappa_0 = \kappa_{1_0} + \delta\kappa_0. \tag{20}$$

It follows from (19) that

$$(D_1 + \Delta D_1)(\kappa_0) = D_1\kappa_{1_0} + (\Delta D_1)(\kappa_{1_0} + \Delta\kappa_0). \tag{21}$$

Consequently,

$$\delta\kappa_0 = \left(\frac{\Delta D_1}{D_1 + \Delta D_1}\right)\Delta\kappa_0. \tag{22}$$

Thus the change $\delta\kappa_0$ in the intrinsic curvature of the composite rod is not identical to the increment $\Delta\kappa_0 = \kappa_{2_0} - \kappa_{1_0}$ in the intrinsic curvature of the laterally accreted mass. Comparing (21) with (12), we can identify $(\Delta D_1)(\kappa_{1_0} + \Delta\kappa_0)$ with K_c. That is, changes to the intrinsic curvature of the composite rod are induced by accretion of material with a different intrinsic curvature. These changes are modeled by κ_c in (11).

4. The governing equations for a single stem

To analyze the predictions of the model, we now restrict attention to a tapered stem of length L which is loaded under its own weight (cf. (7)). In the presence of tip growth, L will increase with time. A vertical force is assumed to be applied at the extremity $s = L$ of the tip:

$$\mathbf{n}(L) = -n_l\mathbf{E}_2. \tag{23}$$

This force often represents the weight imposed at the tip of the rod by additional plant material such as a flower.

We now proceed to integrate $(6)_1$ from an arbitrary point on the branch to the tip $s = L$:

$$\mathbf{n}(L) - \mathbf{n}(s) = \mathcal{P}g\mathbf{E}_2, \tag{24}$$

where

$$\mathcal{P} = \int_L^s -\rho(\bar{s})\mathrm{d}\bar{s}. \tag{25}$$

The contact force $\mathbf{n}$ in the rod can be decomposed into tension n_t and shear n_s forces:

$$n_t = \mathbf{n}(s)\cdot\mathbf{e}_1 = -(\mathcal{P}g + n_l)\sin(\theta), \quad n_s = \mathbf{n}(s)\cdot\mathbf{e}_2 = -(\mathcal{P}g + n_l)\cos(\theta). \tag{26}$$

Where we have used (23).

Using (5), $(6)_{1,2}$, (7), (9), and $(26)_2$, we arrive at the equations of motion:

$$\begin{aligned} \theta' &= v + \kappa_g, \\ v' &= \left(\frac{\mathcal{P}g + n_l}{D(s,t)}\right)\cos(\theta) - \frac{D'(s,t)}{D(s,t)}v, \\ \mathcal{P}' &= -\rho(s,t), \end{aligned} \tag{27}$$

where $D(s,t)$ and $\rho(s,t)$ are prescribed functions of arc-length and time, and the prime $'$ denotes the partial derivative with respect to the arc-length parameter s.

We next substitute the postulated growth law (12) into (27). After some manipulations, a set of differential equations is obtained:

$$\begin{aligned} \theta' &= v + \frac{1}{D(s,t)}\left(D_0\kappa_{g_0} + K_c(s,t) + K_{g_l}(s,t)\right), \\ v' &= \left(\frac{\mathcal{P}g + n_l}{D(s,t)}\right)\cos(\theta) - \frac{D'(s,t)}{D(s,t)}v, \\ \mathcal{P}' &= -\rho(s,t), \\ \dot{K}_c &= \dot{D}(s,t)\left(v(s,t) + \kappa_c(s,t) + \frac{1}{D(s,t)}\left(D_0\kappa_{g_0} + K_c(s,t) + K_{g_l}(s,t)\right)\right), \\ \dot{K}_{g_l} &= D(s,\tau)\dot{\kappa}_{g_l}(s,\tau). \end{aligned} \tag{28}$$

Here, we have used the abbreviations $D_0 = D(s,t_0)$ and $\kappa_{g_0} = \kappa_g(s,t_0)$. Given valid prescriptions for $D(s,t)$ and $\rho(s,t)$, we can prescribe $\kappa_c(s,t)$ and $\kappa_{g_l}(s,t)$ as control inputs to induce plant movement. Alternatively, one can prescribe the motion of the present configuration $\mathcal{L}$ and evolutions $D(s,t)$ and $\rho(s,t)$, and then determine $\kappa_c(s,t)$ and $\kappa_{g_l}(s,t)$.

To determine the spatial location of the rod, we integrate a pair of differential equations:

$$X' = \cos(\theta(s)), \quad Y' = \sin(\theta(s)), \tag{29}$$

using the results from (28). The results of this integration are then used determine the position vector $\mathbf{r} = X\mathbf{E}_1 + Y\mathbf{E}_2$.

5. Growth of a tapered rod

It is constructive to consider the predictions of the model for a tapered rod which is undergoing primary and secondary growth. Both types of growth are illustrated in Fig. 3. We assume that the evolution of κ_g is due to lateral accretion and no remodeling

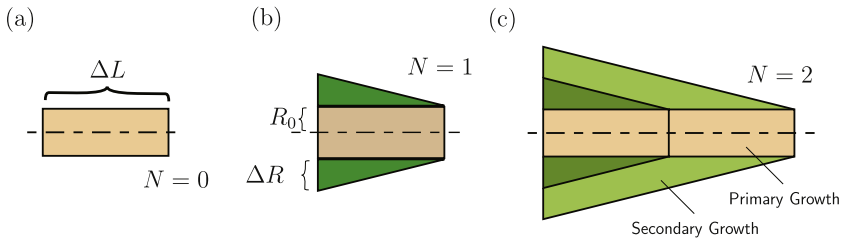

Fig. 3. The process of growth simulated in Cases A, B, and C for two growth steps: $N = 1$ and $N = 2$. The primary growth step length is ΔL with a cylindrical radius of R_0 about the centerline. In addition to primary growth, at each growth step a tapered layer of secondary growth is added to the rod with a thickness of $N\Delta R$ at the base. The rod maintains axial symmetry about the centerline.

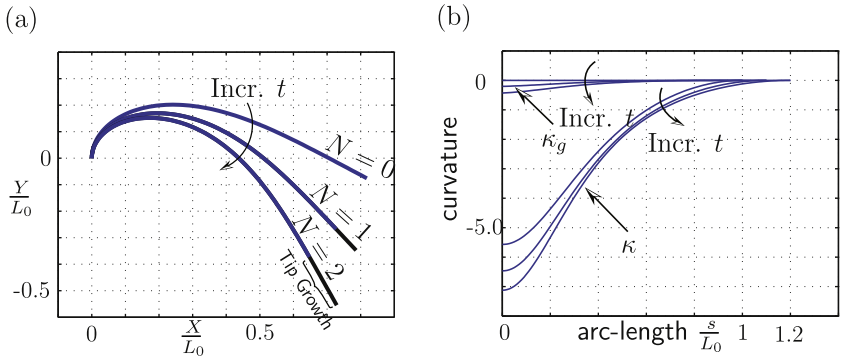

Fig. 4. Three successive simulations of a rod exhibiting tip growth and evolution due to a tapered lateral accretion of material are shown: (a) deformed configurations of the rod and (b) the curvatures κ and κ_g in these configurations. The parameters for the simulation are presented as Case A in Table 1.

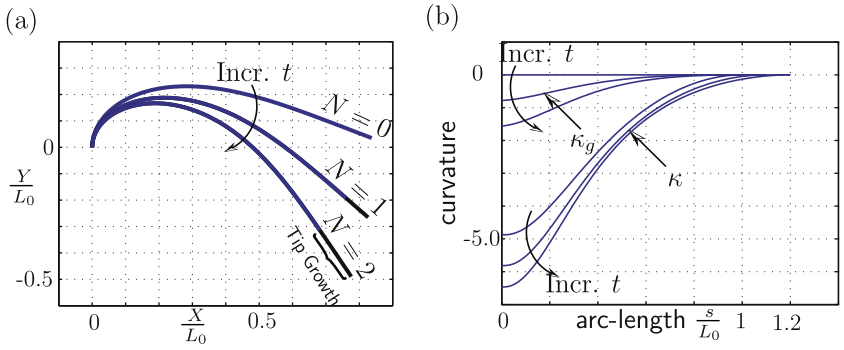

Fig. 5. Three successive simulations of a rod exhibiting tip growth and evolving due to a tapered lateral accretion of material are shown. The parameters for the simulation are presented as Case B in Table 1.

Table 1
The process of growth illustrated in Fig. 3 is simulated for three cases, where E is the modulus of elasticity, ρ^* is density, R_0 is the cylindrical radius of the primary growth segment, ΔR is the vertical thickness of a new added lateral growth layer, L_0 is the initial length of the stem, ΔL is the incremental length of primary growth, F_N is a distributed load on the segment of primary growth, and N is the total number of incremental primary growth segments.

Parameter	Case A	Case B	Case C
E	1.000	1.000	30×10^3 kg/cm^2
ρ^*	4.231	4.231	0.9400 g/cm^3
R_0	1.050 L_0	1.050 L_0	0.1500 cm
ΔR	0.010 L_0	0.050 L_0	0.0241 cm
L_0	–	–	5.0000 cm
ΔL	0.100 L_0	0.100 L_0	5.0000 cm
F_N	0.000	0.000	8.6200 g
N	3	3	11

occurs: $\kappa_c = 0$ and $\kappa_{g_l} = 0$. To this end, three separate sets of simulations for a cantilevered tapered rod are presented. The rod is fixed at $s = 0$ and free at $s = L(t)$, and (28) are integrated numerically using a finite difference method. The parameters for the simulations are shown in Table 1. Cases A and B are both non-dimensionalized simulations with respect to initial length L_0 and are vertically cantilevered at one end ($s = 0$) and free at $s = L$. The third case, Case C, is a dimensionalized simulation, which uses parameters provided by Yamamoto et al. (2002) to recreate a simulation for a progressively grown configuration representing a *Juniperus chinensis* branch.

In Figs. 4 and 5 we show progressive simulations for Cases A and B of the rod growing and evolving due to lateral accretion. The evolution of the intrinsic (growth) curvature κ_g and the change in the curvature κ of the present configuration over time for Cases A and B are shown in Figs. 4 and 5(b), respectively. It is interesting to note that initially $\kappa_g = 0$, but as the rod evolves it rapidly attempts to catch up with κ. By comparing Fig. 4(b) and Fig. 5(b) and referring to Table 1, we can see how a greater change in the stiffness parameter D (Case B having the greater change over time) results in the $\kappa_g \to \kappa$ more rapidly. Case B also has a larger taper, which prevents the present configuration from collapsing as quickly in the downward direction. This structural advantage afforded by the taper is prevalent in many plant structures.

It is instructive to examine the effects of neglecting growth on the deformed shape of the rod. To this end, we consider a tapered rod hanging under gravity. The parameters of the rod are listed as Case C in Table 1, and, to mimic the presence of foliage, a distributed vertical load is also placed along the tip growth region. The rod in its reference configuration is a horizontal line labeled $\mathcal{L}_0$ in Fig. 6. Under the influence of the prescribed forces, the rod will bend downwards. If $\kappa_g = 0$, then the present configuration of the rod is $\mathcal{L}_1$. However, if the rod has intrinsic curvature and a growth configuration $\mathcal{L}_{g_2}$, then the present configuration will be $\mathcal{L}_2$. Clearly, because $\kappa_g \neq 0$, the rod develops a more pronounced deformation.

It is interesting to compare our results for $\mathcal{L}_2$ to a set of results from Yamamoto et al. (2002).[7] One of their results is reproduced in Fig. 6. There are evident qualitative similarities with $\mathcal{L}_2$. What is not apparent from the figure is that the rod model developed in Yamamoto et al. (2002) features an applied moment $\mathbf{m}_a$ which, as discussed in the Appendix A, is intended to model the growth stresses in the

[7] The results from Yamamoto et al. (2002) shown in Fig. 6 correspond to Condition 2-B with the constant $M_1 - m_1$, which describes the differences in the residual stresses between the lower and upper segments of the plant stem, set to 0. In their work, a vertical force was imposed at each 5 cm of the primary growth interval.

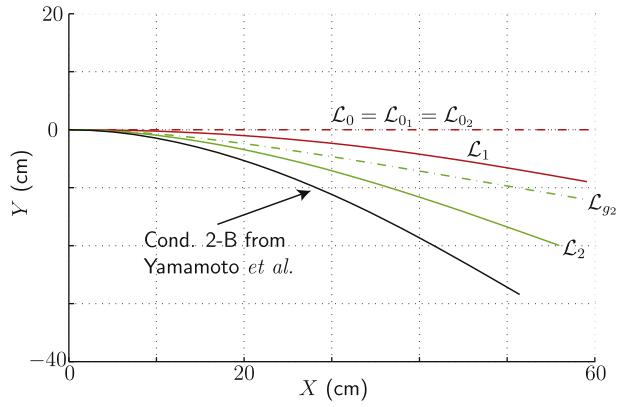

Fig. 6. Simulation results for primary and secondary growth of three tapered rods.

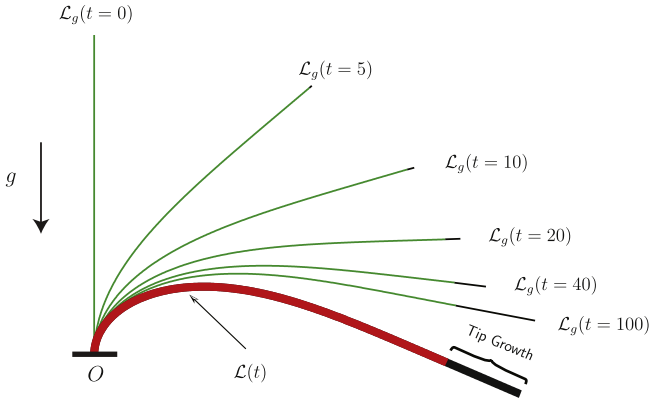

Fig. 7. The present $\mathcal{L}$ configuration of a rod whose stiffness uniformly increases according to (34). During this time period, the rod increases its length by 20% The figure also shows the configurations $\mathcal{L}_g$ of the rod at six distinct instances: $t = [0,5,10,20,40,100]$.

wooded plant, and so is distinct from the rod model we are using in this paper. By varying the parameters associated with $\mathbf{m}_a$, they are able to duplicate the deformed shapes of several plant stems. As will become evident from the results in the next section of this paper, we have also successfully duplicated the shapes of plant stems but without needing to use an applied moment of the form used in Yamamoto et al. (2002).

6. Growth of a tapered rod in the presence of κ_{g_l} and κ_c

Suppose that we are given a sequence of configurations of a plant stem which we then correlate to a sequence of present configurations $\mathcal{L}$ of a rod. Assuming an initial growth configuration, we can solve the inverse problem and deduce κ_c and $\dot{\kappa}_{g_l}$ that will determine the evolution of $\mathcal{L}$ and $\mathcal{L}_g$.

To derive a control law for κ_c and $\dot{\kappa}_{g_l}$ that will allow us to drive the present configuration at an initial time t_0 toward a desired final configuration at time t during the time interval $[t_0,t]$, we prescribe $\kappa(s,\tau)$:

$$\kappa(s,\tau) = f(s,\tau), \quad \tau \in [t_0,t], \quad s \in [0,L(\tau)], \tag{30}$$

where $f = f(s,t)$ is given. Thus,

$$\dot{\kappa}_g = \dot{f} - \dot{\nu}. \tag{31}$$

We can now use the evolution Eq. (11) to solve for κ_c and $\dot{\kappa}_{g_l}$:

$$\dot{D}\kappa_c + D\dot{\kappa}_{g_l} = D(\dot{f} - \dot{\nu}) - \dot{D}\nu. \tag{32}$$

This is the desired general control law. It is easy to see from (32) that if $\dot{D} = 0$ then κ_c has no influence on the evolution of the growth configuration and $\dot{\kappa}_{g_l}$ is the function responsible for the evolution.

Given f and sufficient boundary conditions, we can derive $\theta(s,t)$ and $\kappa(s,t)$ which represent the desired movement of the present configuration. After establishing an initial present configuration, we evolve D and any other prescribed evolution of parameters over an appropriate time interval and solve for the resulting ν using $(27)_{2,3}$:

$$\begin{aligned} \nu' &= \left(\frac{\mathcal{P}g + n_l}{D(s,t)}\right)\cos(\theta) - \frac{D'(s,t)}{D(s,t)}\nu, \\ \mathcal{P}' &= -\rho(s,t). \end{aligned} \tag{33}$$

We then determine $\dot{\nu}$, solve for $\dot{D}\kappa_c + D\dot{\kappa}_{g_l}$ using (32), and solve for the change in κ_g using the relation $\kappa_g = \kappa - \nu$. We now present two demonstrations of these results.

The following is a simple demonstration, shown in Fig. 7, of a constant cross-section uniform rod that undergoes lateral accretion and exhibits tip growth over time. The flexural stiffness is assumed to evolve according to (14) where

$$100\dot{D} + D = 20, \quad D(0) = 1, \quad \rho g = 14. \tag{34}$$

We desire to find $\kappa_c(s,t)$ and $\dot{\kappa}_{g_l}(s,t)$ such that $\dot{\kappa} = 0$ for all time regardless of the change in moment that arises in the present configuration by virtue of the change in $D(s,t)$. As $\dot{f} = 0$, (32) simplifies considerably to

$$\dot{D}\kappa_c + D\dot{\kappa}_{g_l} = -D\dot{\nu} - \dot{D}\nu. \tag{35}$$

That is,

$$-\dot{m} = \dot{D}\kappa_c + D\dot{\kappa}_{g_l} \tag{36}$$

Substituting (35) into (12) and rearranging allows us to compute an expression for $\kappa_g(s,t)$:

$$\begin{aligned} \kappa_g(s,t) = -\nu(s,t) + \frac{D(s,t_0)}{D(s,t)}\left(\kappa_g(s,t_0) + \nu(s,t_0)\right) + \frac{1}{D(s,t)} \\ \times \int_{t_0}^{t} \dot{D}(s,x)\left[\kappa_g(s,x) + \nu(s,x)\right]\mathrm{d}x. \end{aligned} \tag{37}$$

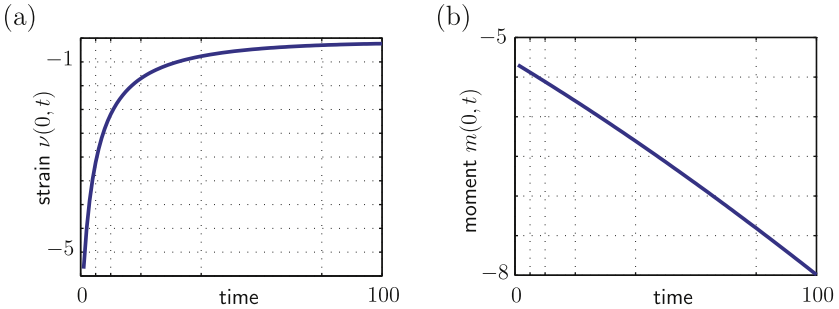

Fig. 8. Graphs of (a) the strain ν and (b) the moment $m = D\nu$ at the base of the rod in Fig. 7 over time.

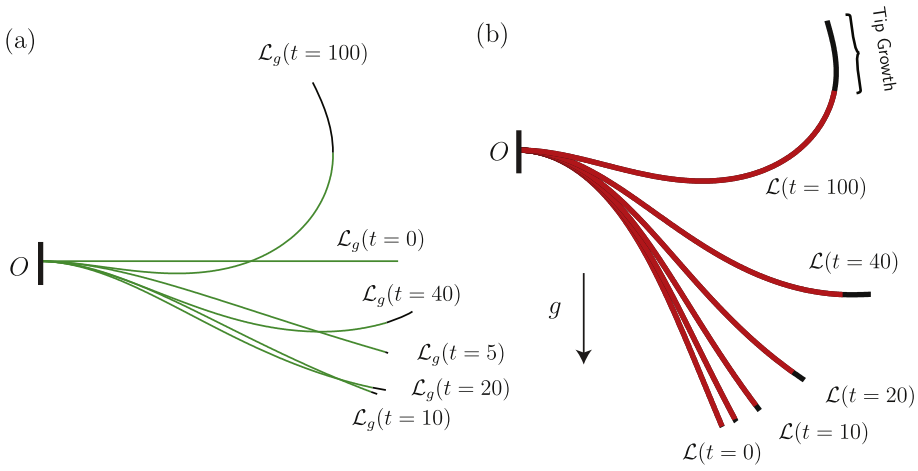

Fig. 9. The (a) growth $\mathcal{L}_g$ and (b) present $\mathcal{L}$ configurations of a rod whose stiffness uniformly increases according to (34) and curvature changes according to (39).

Given $D(s,t)$, there are an infinite number of possible combinations of κ_c and $\dot{\kappa}_{g_l}$ which satisfy (36).

In Fig. 7 we observe that as the tip of the branch grows, the present configuration remains constant. Also, we see that we can capture the phenomenon of the intrinsic curvature profile approaching the present curvature profile. Compared to our earlier work in Faruk Senan et al. (2008) where κ_c and $\dot{\kappa}_{g_l}$ were absent, Fig. 7 exhibits results we are more likely to see in nature when the tip growth rate is appreciable. A measure of the strain $v(0)$ at the base of the rod shown in Fig. 8 reveals that the absolute value of the strain $|v(0)|$ decreases with time. By way of contrast, the moment at the base of the rod $m(0,t) = D(0,t)v(0,t)$, shown in Fig. 8, reveals that the magnitude of the moment $|m(0)|$ increases with time due to the rod's tip growth.

As a second example, we consider a cantilevered rod which at time $t = 0$ hangs under its own weight and whose intrinsic curvature is 0 (see Fig. 9). We then suppose that this rod evolves into the shape of a clothoid over a period of time:

$$\kappa_f = \frac{s}{0.15}. \tag{38}$$

This shape was chosen because of its simplicity and its qualitative similarities to several of the plant stems shown in Niklas and O'Rourke (1982) and Yamamoto et al. (2002). The evolution of $\kappa(t)$ is assumed to be governed by the equation

$$\tau_2\dot{\kappa} + \kappa = \kappa_f, \tag{39}$$

where the relaxation time $\tau_2 = 130$. During the period of transformation, the rod also increases its length by 20% and, paralleling the previous example, changes its stiffness D according to (34). The evolution of the present and growth configurations for this problem are shown in Fig. 9. We believe that this is a convincing example of how changes in κ_g enable the rod to attain the final shape and remain in equilibrium there. The methodology we use here can also be used to simulate plant stem growth where a sequence of recordings of the present configurations of the plant stem are available.

7. Closing comments

The evolution Eq. (11) addresses several limitations present in the earlier developments of Faruk Senan et al. (2008). With the appropriate rod theory, it can be used to mimic the growth and evolution of plant stems and related equations can readily be postulated for more elaborate rod theories which capture torsion and transverse shear. Despite these capabilities, the main issue with (11) is the substantial hurdle in correlating κ_c and κ_{g_l} to biochemical stimuli, such as auxins, which govern the growth of plants. This difficulty is present for most growth models in biomechanics. One step towards surmounting this challenge, and the topic of future work, features the inverse method discussed in Section 6. With the help of this method, it is possible to take data on the evolution of the curvature, flexural rigidity and density of a plant stem and use it to infer the functions κ_c and κ_{g_l}.

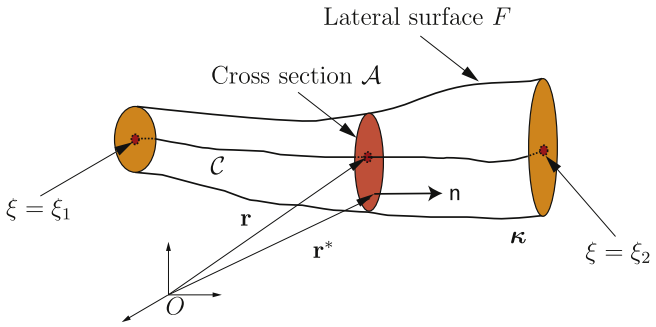

Fig. A.10. Schematic of the present configuration $\boldsymbol{\kappa}$ of a rod-like body $\mathcal{B}$.

Acknowledgements

The authors would like to take this opportunity to thank Prof. Jerry Sackman (U. C. Berkeley) for helpful remarks on composite rods and Prof. Wendy Silk (U. C. Davis) for her valuable comments on plant growth. During his graduate studies at the University of California at Berkeley, Timothy Tresierras was supported as a Sloan Scholar.

Appendix A. Rod theories, residual forces, and residual moments

In this Appendix, we address the issue of residual forces $\overset{o}{\mathbf{n}}$ and residual moments $\overset{o}{\mathbf{m}}$ in certain rod theories. Due to the importance of a type of residual stress which is known as growth stress in the mechanics of plants, the correspondence between $\overset{o}{\mathbf{n}}$ and $\overset{o}{\mathbf{m}}$ and the residual stress field $\overset{o}{\mathbf{T}}$ in the body that the rod is modeling are discussed. In particular, a criterion is presented to distinguish cases where $\overset{o}{\mathbf{n}}$ and $\overset{o}{\mathbf{m}}$ are compatible with $\overset{o}{\mathbf{T}}$. This criterion is shown to

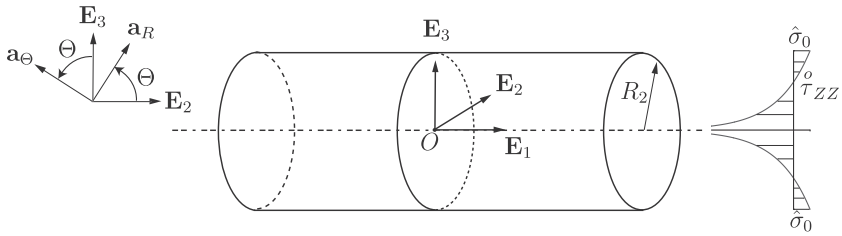

Fig. A.11. Schematic of the present configuration section of a plant stem illustrating bases vectors (A.6) and a component $\overset{o}{\tau}_{ZZ}$ of Kübler's residual stress field (A.8).

be satisfied by a classical prescription of $\overset{o}{\mathbf{T}}$ due to Kübler (1959a,b), but not by a more recent prescription by Yamamoto et al. (2002).

For a body $\mathcal{B}$, the residual (Cauchy) stress tensor $\overset{o}{\mathbf{T}}$ is the stress field remaining in a stationary present configuration after applied tractions to its boundary and body forces have been removed. The stress field satisfies the equilibrium equations and boundary conditions:

$$\operatorname{div}\left(\overset{o}{\mathbf{T}}\right)=\mathbf{0},\quad \overset{o}{\mathbf{T}}\mathsf{n}=\mathbf{0}, \tag{A.1}$$

where n is the unit outward normal to the boundary of $\mathcal{B}$ in its present configuration.[8]

For a rod, the residual force $\overset{o}{\mathbf{n}}$ and residual moment $\overset{o}{\mathbf{m}}$ satisfy the balance laws subject to a set of trivial boundary conditions:

$$\begin{aligned}&\overset{o}{\mathbf{n}}(\xi_{1,2},t)=\mathbf{0},\quad \overset{o}{\mathbf{m}}(\xi_{1,2},t)=\mathbf{0},\\ &\frac{\partial\overset{o}{\mathbf{n}}}{\partial\xi}=\mathbf{0},\quad \frac{\partial\overset{o}{\mathbf{m}}}{\partial\xi}+\frac{\partial\mathbf{r}}{\partial\xi}\times\overset{o}{\mathbf{n}}=\mathbf{0}.\end{aligned} \tag{A.2}$$

Here, the material curve $\mathcal{C}$ is parameterized by the convected coordinate $\xi\in[\xi_1,\xi_2]$. The Eq. (A.2) are the static equilibrium equations for the rod in the absence of applied forces, applied moments, terminal forces, and terminal moments (cf. (6)). It is easy to argue with the help of (A.2) that, for $\xi\in[\xi_1,\xi_2]$,

$$\overset{o}{\mathbf{n}}(\xi,t)=\mathbf{0},\quad \overset{o}{\mathbf{m}}(\xi,t)=\mathbf{0}. \tag{A.3}$$

Consequently, the residual forces and residual moments in a rod vanish. Our discussion here applies not only to Euler's elastica but also the more elaborate Kirchhoff–Love rod theory.

There is a direct correspondence between the rod theories of interest in this paper and three-dimensional continuum mechanics. The present configuration $\boldsymbol{\kappa}$ of a rod-like body $\mathcal{B}$ is shown in Fig. A.10. We follow Green and Naghdi (1979) and note that in order to model this body using a rod theory, we approximate the centerline of the body using the material curve $\mathcal{C}$. The lateral surface of $\mathcal{B}$ is approximated by the surface F. At each point ξ of $\mathcal{C}$ we can define a cross section $\mathcal{A}$ and the position vector of a point on $\mathcal{A}$ relative to $\mathcal{C}$ is defined by the vector $\mathbf{r}^*-\mathbf{r}$. With these preliminaries aside, we now recall from Green and Naghdi (1979), the identifications for some of the fields appearing in the balance laws (6) and (A.2)[9]:

$$\mathbf{n}=\int_{\mathcal{A}}\mathbf{T}\mathsf{n}da,\quad \mathbf{m}=\int_{\mathcal{A}}(\mathbf{r}^*-\mathbf{r})\times\mathbf{T}\mathsf{n}da, \tag{A.4}$$

where n is the unit outward normal to $\mathcal{A}$.

With the help of (A.4), we can establish a criterion for the compatibility of a residual stress tensor $\overset{o}{\mathbf{T}}$ with the corresponding quantities in a rod theory. As $\overset{o}{\mathbf{n}}$ and $\overset{o}{\mathbf{m}}$ are identically zero, we find that

$$\int_{\mathcal{A}}\overset{o}{\mathbf{T}}\mathsf{n}da=\mathbf{0},\quad \int_{\mathcal{A}}(\mathbf{r}^*-\mathbf{r})\times\overset{o}{\mathbf{T}}\mathsf{n}da=\mathbf{0}, \tag{A.5}$$

We refer to residual stress fields which satisfy (A.5) as compatible. It is instructive to turn to two examples: one of which will prove to be compatible.

The first example can be found in many treatments of residual stress in plant stems (see Archer (1986) and references cited therein). Here, we consider a segment of a plant stem which is in the form of a cylinder (see Fig. A.11). The outer radius R_2 of the plant stem increases in time due to secondary growth featuring accretion of outer layers. These growth layers subsequently swell or shrink in the longitudinal, radial and tangential directions and this induces surface stresses in the growth layers. The surface stresses that are produced contribute to the residual stress field $\overset{o}{\mathbf{T}}$ in the plant stem. To analyze $\overset{o}{\mathbf{T}}$, it is traditional to restrict attention to infinitesimal displacements and use a cylindrical polar coordinate system (R,Θ,Z) for $\boldsymbol{\kappa}$. We identify Z with ξ and define an orthonormal triad:

$$\begin{aligned}&\mathbf{a}_R=\cos(\Theta)\mathbf{E}_2+\sin(\Theta)\mathbf{E}_3,\\ &\mathbf{a}_\Theta=-\sin(\Theta)\mathbf{E}_2+\cos(\Theta)\mathbf{E}_3,\\ &\mathbf{a}_Z=\mathbf{E}_1.\end{aligned} \tag{A.6}$$

Note that the axis of the plant stem is parallel to the $\mathbf{E}_1$ vector and that the cross sections of the plant stem lie in the X_2-X_3 plane. After some elementary manipulations with (A.4) it can be shown that

$$\begin{aligned}&\mathbf{n}=\int_{\mathcal{A}}(\tau_{ZR}\mathbf{a}_R+\tau_{Z\Theta}\mathbf{a}_\Theta+\tau_{ZZ}\mathbf{a}_Z)RdRd\Theta,\\ &\mathbf{m}=\int_{\mathcal{A}}(\tau_{Z\Theta}\mathbf{a}_3-\tau_{ZZ}\mathbf{a}_\Theta)R^2dRd\Theta,\end{aligned} \tag{A.7}$$

where $\tau_{Z\Theta}$, τ_{ZZ}, and τ_{ZR} are components of $\mathbf{T}$.

Assuming that the plant stem is composed of a transversely isotropic material, Kübler (1959a,b) has shown that the residual stresses of interest here are[10]

$$\overset{o}{\tau}_{ZZ}=\hat{\sigma}_0\left(1+2\log\left(\frac{R}{R_2}\right)\right),\quad \overset{o}{\tau}_{ZR}=0,\quad \overset{o}{\tau}_{Z\Theta}=0, \tag{A.8}$$

where R_2 is the outer radius of the stem and $\hat{\sigma}_0$ is a constant which is determined by the strains on the lateral surface of the stem. Substituting (A.8) into (A.7), integrating and ornamenting the resulting values of $\mathbf{n}$ and $\mathbf{m}$ with tildes, we find that $\tilde{\mathbf{n}}=\mathbf{0}$ and $\tilde{\mathbf{m}}=\mathbf{0}$. This result is consistent with (A.3) and we conclude that Kübler's residual stress field is compatible.

In Yamamoto et al. (2002, Eqs. (23)–(26)), the expression for $\overset{o}{\tau}_{ZZ}$ in (A.8) is replaced by an expression which depends on Θ and is independent of R:

[8] Discussions on methods for finding the solution $\overset{o}{\mathbf{T}}$ to these equations can be found in Johnson and Hoger (1995) and Hoger (1986).

[9] Related discussions of these prescriptions can be found in Antman (2005) and Rubin (2000).

[10] See Archer (1986, p.76).

$$\overset{o}{\tau}_{ZZ} = \sigma_0 + \left(\sigma_0 - \frac{M_1 + m_1}{2} - \left(\frac{M_1 - m_1}{2}\right)\cos(\Theta)\right)\sin(\theta - \theta_P), \tag{A.9}$$

where M_1, m_1, σ_0 are constants and θ_P is a "preferred" angle of tip growth. Omitting details in the interests of brevity, we find that $\tilde{\mathbf{n}} \neq \mathbf{0}$ and $\tilde{\mathbf{m}} \neq \mathbf{0}$. Consequently, the residual stress field is incompatible and (A.9) cannot be modeled by residual forces and residual moments in a rod. Indeed in Yamamoto et al. (2002), the resulting expression for $\tilde{\mathbf{m}}$ defines an applied moment $\mathbf{m}_a$ acting on the rod.

References

Alford, P.W., Humphrey, J.D., Taber, L.A., 2008. Growth and remodeling in a thick-walled artery model: effects of spatial variations in wall constituents. Biomech. Model. Mechanobiol. 7 (4), 245–262. URL <http://dx.doi.org/10.1007/s10237-007-0101-2>.

Alméras, T., Gril, J., Costes, E., 2002. Bending of apricot tree branches under the weight of axillary growth: test of a mechanical model with experimental data. Trees 16 (1), 5–15. URL <http://dx.doi.org/10.1007/s00468-001-0139-1>.

Antman, S., 2005. Nonlinear Problems of Elasticity, second ed. Springer-Verlag, New York.

Archer, R.R., 1986. Growth Stresses and Strains in Trees. Springer-Verlag, Berlin.

Costes, E., Smith, C., Renton, M., Guédon, Y., Prusinkiewicz, P., Godin, C., 2008. MAppleT: simulation of apple tree development using mixed stochastic and biomechanical models. Funct. Plant Biol. 35 (9–10), 936–950. URL <http://dx.doi.org/10.1071/FP08081>.

Faruk Senan, N.A., O'Reilly, O.M., Tresierras, T.N., 2008. Modeling the growth and branching of plants: a simple rod-based model. J. Mech. Phys. Solids 56 (10), 3021–3036. URL <http://dx.doi.org/10.1016/j.jmps.2008.06.005>.

Fourcaud, T., Blaise, F., Lac, P., Castéra, P., de Reffye, P., 2003. Numerical modelling of shape regulation and growth stresses in trees I. Implementation in the AMAPpara software and simulation of tree growth. Trees 17 (1), 31–39. URL <http://dx.doi.org/10.1007/s00468-002-0203-5>.

Fourcaud, T., Lac, P., 2003. Numerical modelling of shape regulation and growth stresses in trees I. An incremental static finite element formulation. Trees 17 (1), 23–30. URL <http://dx.doi.org/10.1007/s00468-002-0202-6>.

Fournier, M., Bordonné, P.A., Guitard, D., Okuyama, T., 1990. Growth stress patterns in tree stems: a model assuming evolution with the tree age of maturation strains. Wood Sci. Technol. 24 (2), 131–142. URL <http://dx.doi.org/10.1007/BF00229049>.

Fung, Y.C., 1991. What are the residual stresses doing in our blood vessels? Ann. Biomed. Eng. 19 (3), 237–249. URL <http://dx.doi.org/10.1007/BF02584301>.

Goriely, A., Goldstein, R.E., 2006. Dynamic buckling of morphoelastic filaments. Phys. Rev. E. 74 (1). URL <http://dx.doi.org/10.1103/PhysRevE.74.010901>.

Goriely, A., Neukirch, S., 2006. Mechanics of climbing and attachment in twining plants. Phys. Rev. Lett. 97 (18). URL <http://dx.doi.org/10.1103/PhysRevLett.97.184302>.

Green, A., Naghdi, P., 1979. On thermal effects in the theory of rods. Int. J. Solids Struct. 15 (11), 829–853. URL <http://dx.doi.org/10.1016/0020-7683(79)90053-2>.

Green, A.E., Naghdi, P.M., 1995. A unified procedure for construction of theories of deformable media. II. Generalized continua. Proc. Roy. Soc. Lond. Ser. A 448 (1934), 357–377. URL <http://dx.doi.org/10.1098/rspa.1995.0021>.

Greenhill, A.G., 1881. Determination of the greatest height consistent with stability that a vertical pole or mast can be made, and of the greatest height to which a tree of given proportions can grow. Proc. Camb. Phil. Soc. 4, 65–73.

Hoger, A., 1986. On the determination of residual stress in an elastic body. J. Elast. 16 (3), 303–324. URL <http://dx.doi.org/10.1007/BF00040818>.

Johnson, B.E., Hoger, A., 1995. The use of a virtual configuration in formulating constitutive equations for residually stressed elastic materials. J. Elast. 41 (3), 177–215. URL <http://dx.doi.org/10.1007/BF00041874>.

Kübler, H., 1959a. Studies on growth stresses in trees – Part 1: The origin of growth stresses and the stresses in transverse direction. Eur. J. Wood Wood Prod. 17 (1), 1–9. URL <http://dx.doi.org/10.1007/BF02608827>.

Kübler, H., 1959b. Studies on growth stresses in trees - Part 2: Longitudinal stresses. Eur. J. Wood Wood Prod. 17 (2), 44–54. URL <http://dx.doi.org/10.1007/BF02626321>.

Love, A.E.H., 1944. A Treatise on the Mathematical Theory of Elasticity. Dover Publications, Inc., New York.

McMillen, T., Goriely, A., 2002. Tendril perversion in intrinsically curved rods. J. Nonlinear Sci. 12 (3), 241–281. URL <http://dx.doi.org/10.1007/s00332-002-0493-1>.

Niklas, K.J., O'Rourke, T.D., 1982. Growth patterns of plants that maximize vertical growth and minimize internal stresses. Amer. J. Bot. 69 (9), 1367–1374. URL <http://www.jstor.org/stable/2443098>.

O'Reilly, O.M., 2007. A material momentum balance law for rods. J. Elast. 86 (2), 155–172. URL <http://dx.doi.org/10.1007/s10659-006-9089-6>.

O'Reilly, O.M., Varadi, P.C., 2003. On energetics and conservations for strings in the presence of singular sources of momentum and energy. Acta Mech. 165 (1–2), 27–45. URL <http://dx.doi.org/10.1007/s00707-003-0032-7>.

Ormarsson, S., Dahlblom, O., Johansson, M., 2009. Finite element study of growth stress formation in wood and related distortion of sawn timber. Wood Sci. Technol. 43 (5–6), 387–403. URL <http://dx.doi.org/10.1007/s00226-008-0209-2>.

Rubin, M.B., 2000. Cosserat Theories: Shells, Rods, and Points. Kluwer Academic Press, Dordrecht.

Silk, W., Wang, L., Cleland, R., 1982. Mechanical properties of the rice panicle. Plant Phys. 70 (2), 460–464. URL <http://www.plantphysiol.org/cgi/content/abstract/70/2/460>.

Silk, W.K., Erickson, R.O., 1980. Kinematics of plant growth. Sci. Amer. 242 (5), 134–151.

Taber, L.A., 1995. Biomechanics of growth, remodeling, and morphogenesis. ASME Appl. Mech. Rev. 48 (8), 487–545. URL <http://dx.doi.org/10.1115/1.3005109>.

Taber, L.A., 2009. Towards a unified theory for morphomechanics. Philos. Trans. R. Soc. Lond. Ser. A Math. Phys. Eng. Sci. 367 (1902), 3555–3583. URL <http://dx.doi.org/10.1098/rsta.2009.0100>.

Wilson, B.F., Archer, R.R., 1977. Reaction wood: Induction and mechanical action. Ann. Rev. Plant Physiol. 28, 23–43. URL <http://dx.doi.org/10.1146/annurev.pp.28.060177.000323>.

Yamamoto, H., Yoshida, M., Okuyama, T., 2002. Growth stress controls negative gravitropism in woody plant stems. Planta 216 (2), 280–292. URL <http://dx.doi.org/10.1007/s00425-002-0846-x>.